Article

Geochemical Investigations of Fe-Si-Mn Oxyhydroxides Deposits in Wocan Hydrothermal Field on the Slow-Spreading Carlsberg Ridge, Indian Ocean: Constraints on Their Types and Origin

Samuel Olatunde Popoola [1,2,3] ![ORCID], **Xiqiu Han** [1,2,*] ![ORCID], **Yejian Wang** [1] ![ORCID], **Zhongyan Qiu** [1] **and Ying Ye** [2]

1   Key Laboratory of Submarine Geosciences, Second Institute of Oceanography, State Oceanic Administration, Hangzhou 310012, China; lekpopesam@yahoo.com (S.O.P.); yjwang@sio.org.cn (Y.W.); qiuzy@sio.org.cn (Z.Q.)
2   Department of Marine Science, Ocean College, Zhejiang University, Zhoushan 316021, China; gsyeying@zju.edu.cn
3   Nigerian Institute for Oceanography and Marine Research, Lagos P.M.B 12729, Nigeria
*   Correspondence: xqhan@sio.org.cn

![check for updates]

Abstract: We have studied morphology, mineralogy and geochemical characteristics of Fe-oxyhydroxide deposits from metal-enriched sediments of the active (Wocan-1) and inactive (Wocan-2) hydrothermal sites (Carlsberg Ridge, Northwest Indian Ocean). Fe-oxyhydroxide deposits on the Wocan-1 site are reddish-brownish, amorphous and subangular. They occur in association with sulfides (e.g., pyrite, chalcopyrite and sphalerite) and sulfate minerals (e.g., gypsum and barite). The geochemical composition shows enrichment in transition metals (Σ (Cu + Co + Zn + Ni) = ~1.19 wt. %) and low (<0.4 wt. %) values of Al/(Al + Fe + Mn) ratio. The Wocan-2 samples show poorly crystallized reddish brown and yellowish Fe-oxyhydroxide, with minor peaks of goethite and manganese oxide minerals. The mineral assemblage includes sulfide and sulfate phases. The geochemical compositions show two distinct types (type-1 and type-2). The type-1 Fe-oxyhydroxides are enriched in transition metals (up to ~1.23 wt. %), with low values of Fe/Ti vs. Al/(Al + Fe + Mn) ratio similar to the Wocan-1 Fe-oxyhydroxides. The type-2 Fe-oxyhydroxides are depleted in transition metals, with Al/(Al + Fe + Mn) ratio of 0.003–0.58 (mean value, 0.04). The ridge flank oxyhydroxides exhibit an extremely low (mean value ~ 0.01) Fe/Mn ratio and a depleted concentration of transition metals. Our results revealed that the Wocan-1 Fe-oxyhydroxides and type-1 Fe-oxyhydroxides of the Wocan-2 site are in the range of Fe-oxyhydroxides deposits that are precipitated by mass wasting and corrosion of pre-existing sulfides. The type-2 Fe-oxyhydroxides are precipitated from sulfide alteration by seawater in an oxygenated environment relative to type-1. The association of biogenic detritus with the oxyhydroxides of the ridge flanks and the low Fe/Mn ratio suggests hydrogenous/biogenic processes of formation and masked hydrothermal signatures with distance away from the Wocan hydrothermal field.

Keywords: geochemistry; Fe-oxyhydroxides; metalliferous sediments; Wocan Hydrothermal Field; Carlsberg Ridge; Indian Ocean.

1. Introduction

Fe-Si-Mn oxide mineral deposits are formed in various geologic settings such as mid-ocean ridges MOR [1–3]; back-arc spreading centers [4–7]; submerged island arc volcanoes and hot-spot-associated volcanic intraplate [8–12]. They are essential components of modern seafloor deposits [12] and generally occur in the form of sulfide oxidation (e.g., gossan/ferruginous ochre from the sulfide mound at the Trans-Atlantic Geotraverse (TAG) hydrothermal site) [2] and primary precipitations from hydrothermal fluid (e.g., chimneys, mounds and ochres formation in the TAG field) [13]. Others also occur in the form of crack fills or interstitial precipitates [1,14].

Fe-oxyhydroxides are precipitated into the near active and inactive vent sediments due to the erosion of dispersed coarse-grained oxyhydroxide particles that are deposited a few hundreds of meters from hydrothermal sites. Whereas, fine-grained particles are liable to be dispersed by bottom currents to tens of kilometers into the ridge flanks as plume fall-out [2].

Previous reports have identified four distinct types of Fe-oxides and hydroxides by geochemical compositions, tectonism and mineralization [1,2,12,14,15]. The first group of oxyhydroxides deposits displays the depleted concentration of transition metals (e.g., <0.05 wt. % and Fe content ranges of 27~45 wt. %). Their formation was related to the reaction between descending cold seawater and ascending hot hydrothermal fluid [1,14,16]. (ii) The second group displays the increased concentration of transition metals (e.g., >0.4–1 wt. % and Fe content ranges of 30–50 wt. %). Their formation was related to the secondary oxidation of hydrothermal sulfides [12,14,16]. (iii) The third group displays depleted transition metals, with variable Fe (20–30 wt. %), Si (7–20 wt. %) contents and enriched clay minerals. Whereas, the fourth group displays depleted concentration of transition metals, low Fe (<10 wt. %), high Si (>35 wt. %) and enriched opaline silica [14]. Moreover, References [15,17] also related the influence and activities of microorganisms (e.g., iron-oxidizing chemosynthetic bacteria) to the formation of typical Fe-oxyhydroxide deposits in the Lau Basin and Eastern Manus Basin.
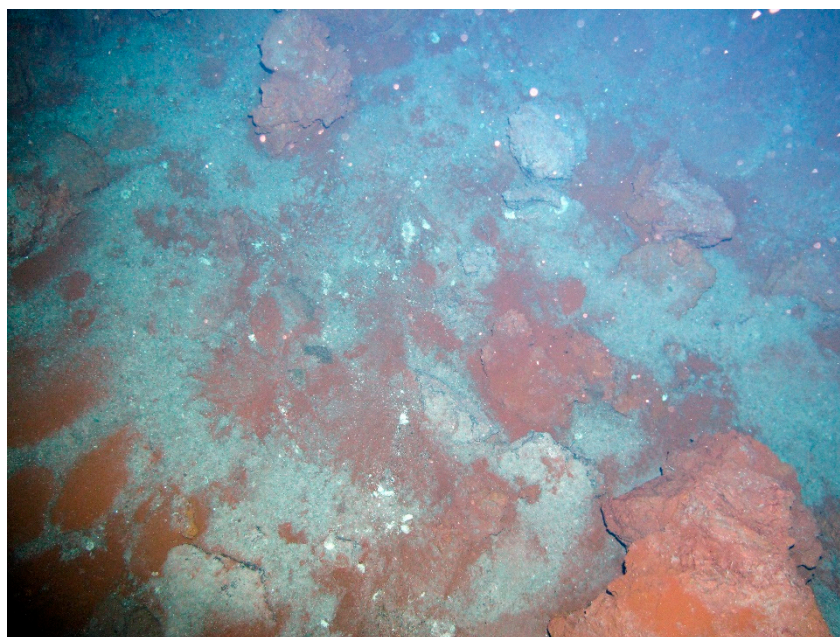
Studies on Fe-oxyhydroxide deposits in the Indian Ocean Ridge systems are few. Recent studies are the work of [18] from Southwest Indian Ridge (SWIR). Hydrothermal plume particles and polymetallic samples that are enriched in metal content were discovered within the Carlsberg Ridge, northwest Indian Ocean during the Chinese DY 28th cruise in 2013 (near $6^{\circ}22'$ N/$60^{\circ}31'$ E and referred to as Wocan Hydrothermal Field (WHF) [19]). These particles indicate the presence of an active hydrothermal system (Wocan-1), together with the inactive sulfide chimney (Wocan-2) that are related to widespread past venting [19]. Additionally, Reference [19] reported the occurrence of iron-oxyhydroxides together with atacamite in the form of vugs lining in the interstitial spaces of the Cu-rich chimney on the Wocan-1 hydrothermal site. However, studies on the origin, morphology and mineral chemistry of Fe oxides and hydroxide deposits of the Wocan field had not been conducted. This present study examines the morphology and chemical compositions of Fe-oxyhydroxide mineral grains separated from metalliferous sediments of the WHF. We aim to understand the probable origin, types and modes of precipitation of Fe-oxides and hydroxide deposits of the Wocan and the ridge flanks.

2. Sampling Stations and Study Area

The Wocan Hydrothermal Field (Figure 1), is a basalt-hosted hydrothermal site, formed on a neo-volcanic ridge [19,20]. The Wocan-1 site covers an area of ~420 m by 320 m in the water depth between 2970~2990 m. The Wocan-2 site covers an area of 420 m by 120 m, located at a water depth ~3100 m, ~2.7 km northwest to Wocan-1 [19]. Sediment samples were collected from six stations in the Carlsberg Ridge, which include (i) active hydrothermal site (station 28I-TVG07 and 28I-TVG08, Figure 2). (ii) Inactive hydrothermal site (station 28I-TVG10 and 28II-TVG05) and (iii) ridge flanks (station 28I-TVG12 and 28I-TVG13).
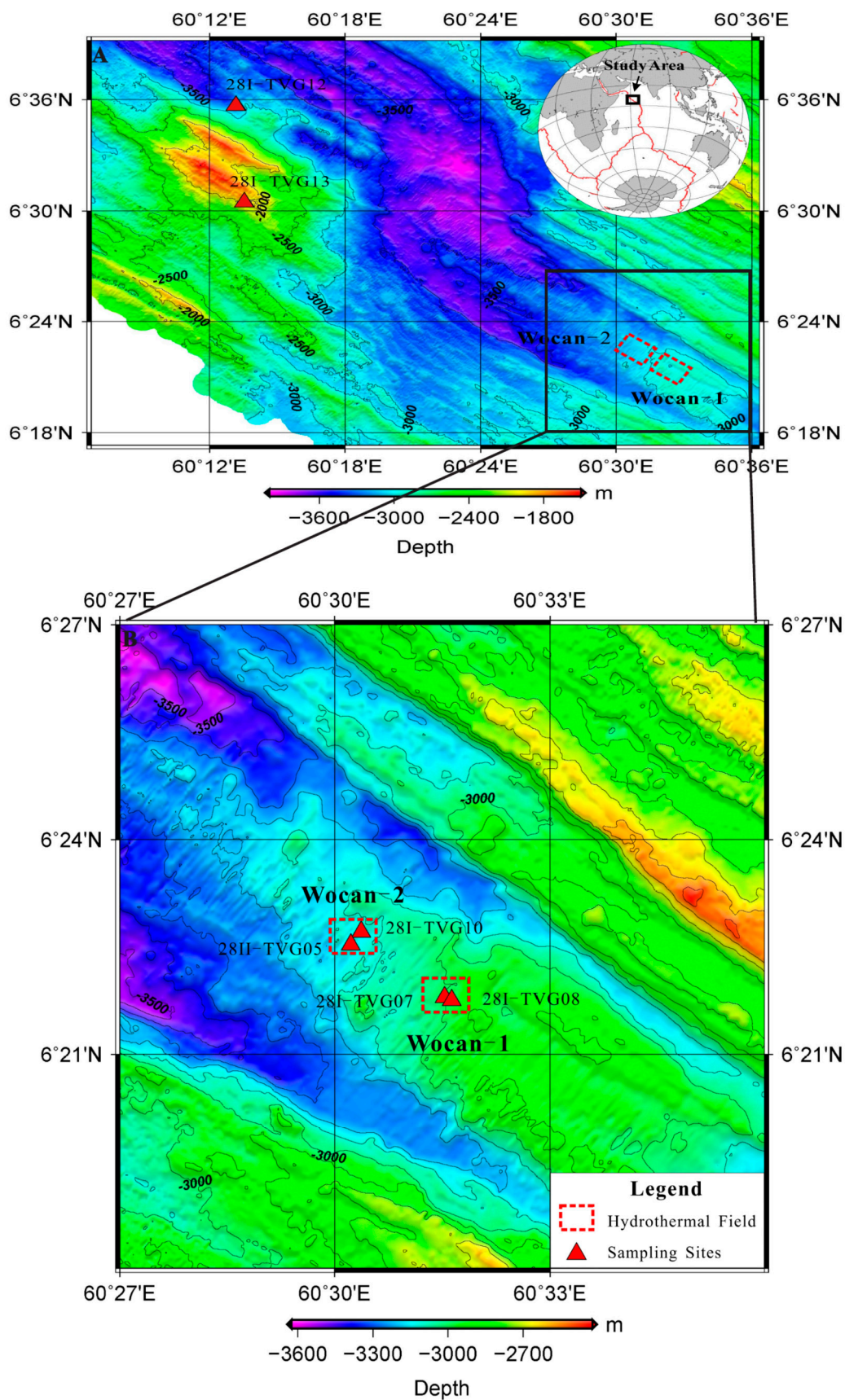
Figure 1. Bathymetric map of (**A**) showing the locations of Wocan-1 and Wocan-2 hydrothermal sites and the sampling stations in the ridge flank; (**B**) The enlarged map of A showing the sampling stations in Wocan-1 and Wocan-2 hydrothermal field.

Figure 2. Fe-oxyhydroxide deposits in the Wocan-1 hydrothermal site (station 28I-TVG08).

3. Materials and Methods

Metalliferous sediments were sampled by TV-grab sampler at six stations during the DY 28th cruise in 2013 (Table 1). Rock fragments that are too large for grain mount were isolated from the samples under the binocular microscope. Representative samples from each station were washed with ultra-pure water to remove interstitial salts, dried at 60 °C and weighed. Approximately 50 g were wet-sieved and separated into >63 μm and <63 μm (silt and clay size fraction) using 240 mesh sizes. From the sieved (>63 μm) fractions, Fe-oxyhydroxide grains were examined and hand-picked under the stereographic and binocular microscope. Micromorphological observations were conducted on the separated grains with Leica M205C stereographic microscope in combination with a scanning electron microscope (SEM) equipped with Energy Dispersive Spectrometer (EDS) analytical X-ray system. The SEM-EDS was operated at an accelerating voltage of 20 kV and a beam current of 16–22 mA at the State Key Laboratory of Submarine Geosciences (KLSG), Hangzhou, China. The isolated Fe-oxyhydroxide grains were then impregnated with epoxy resin and hardener (ratio 2:1), similar to the method of [21] and polished. Chemical compositions of Fe-oxyhydroxide grain separates were performed on a JEOL JXA-8100 Superprobe Electron Probe Microanalysis (EPMA) at 15 kV acceleration voltage with a beam current of $\sim 2 \times 10^{-8}$ A and beam size of 5μm at KSLG. A 10–20 nm thick carbon layer was coated on the samples, before EPMA investigation. The standard used include synthetic oxide set (K_2O, FeO, MnO_2, TiO_2, Cr_2O_3) for K, Fe, Mn, Ti and Cr respectively. Others include: apatite for Ca and P, barite for Ba and S; olivine for Mg and Na; $SrSO_4$ for S. ZAF correction program was employed according to the method of [22]. The results are documented with photomicrographs and micro-chemical compositions of the phases. EPMA concentrations of individual analyses are given in Supplementary Materials, with a detection limit of >0.01 wt. % and analytical precision of <10%.

Furthermore, the traditional method of counting was adopted on ~250 to 260 randomly counted grains at the six stations. The grains were temporarily mounted on stud attached with carbon tapes to a set of slides using a pre-cleaned needle with methylated spirit according to [23]. Fe-oxyhydroxide grains were counted in order to have an idea about its relative abundance at the six sampling stations.

Also, bulk-X-ray powder diffraction analysis (XRD) was conducted on the part of the sediment after grinding ~2 g of representative samples from each station in an agate mortar and pestle. The XRD analysis was investigated using X-Pert PRO Diffractometer, with Cu *kα* radiation generated at 45 kV and 40 mA and a beam diameter of 0.1 mm at KSLG.

Table 1. The sampling information of studied bulk samples.

| Site	Station	Longitude (E)	Latitude (N)	Depth (m)
Wocan-1	28I-TVG07	60°31.534′	6°21.796′	2989
	28I-TVG08	60°31.635′	6°21.756′	2973
Wocan-2	28I-TVG10	60°30.372′	6°21.866′	3104
	28II-TVG05	60°30.226′	6°22.534′	3105
Ridge Flank	28I-TVG13	60°13.190′	6°35.675′	3254
	28I-TVG12	60°13.550′	6°30.462′	2009

## 4. Results

4.1. Bulk Sediment Mineralogy

The bulk mineralogy of representative sediment fractions of Wocan-2 when compared with the standard according to [24], suggests a minor and weak goethite peak characterized by different diffraction patterns. These patterns are with d-spacing of 1.8041Å (50.550); 1.6922Å (54.154); 2.583Å (34.7° 2θ); 2.450 Å (36.6° 2θ); 2.253 Å (39.9° 2θ); 3.383 Å (26.3° 2θ) and 4.183 Å (21.2° 2θ) (Figure 3 and 4). The characteristic diffraction patterns with d-spacings of 1.564Å (58.7° 2θ) and 2.568 Å (34.9° 2θ) and its comparison with appropriate standard according to [25] suggests manganosite (manganese oxide minerals, Figure 4).

The Wocan-1 samples are generally amorphous, with a non-identifiable peak of Fe-oxides and hydroxides. Other characteristic XRD patterns suggest sulfide minerals (e.g., sphalerite, chalcopyrite and pyrite) and associated sulfate mineral minerals (gypsum and barite). We have reported the detailed information on the sulfide mineral separates in Reference [26].

The bulk mineralogy of the representative sediment fractions of the ridge flank is dominated by biogenic calcite (mainly foraminifera assemblage) and traces of phyllosilicate minerals vermiculites (Figure 5). Optical microscopy and SEM-EDS investigation also revealed the presence of a minor abundance of Fe-oxyhydroxide grains (Table 2).
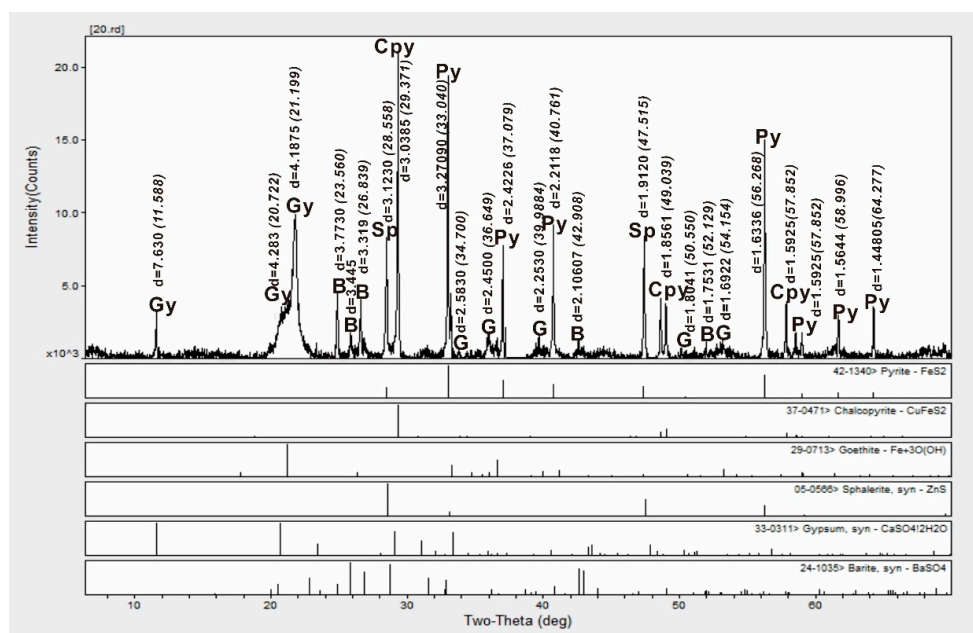
Figure 3. XRD patterns of the bulk sediment from the station 28I-TVG10 (Wocan-2 site). Abbreviations, G: goethite; Gy: gypsum; B: Barite; Sp: sphalerite; Cpy: chalcopyrite; Py: pyrite. The 2θ values are enclosed in the bracket, whereas, the first values are the d values.
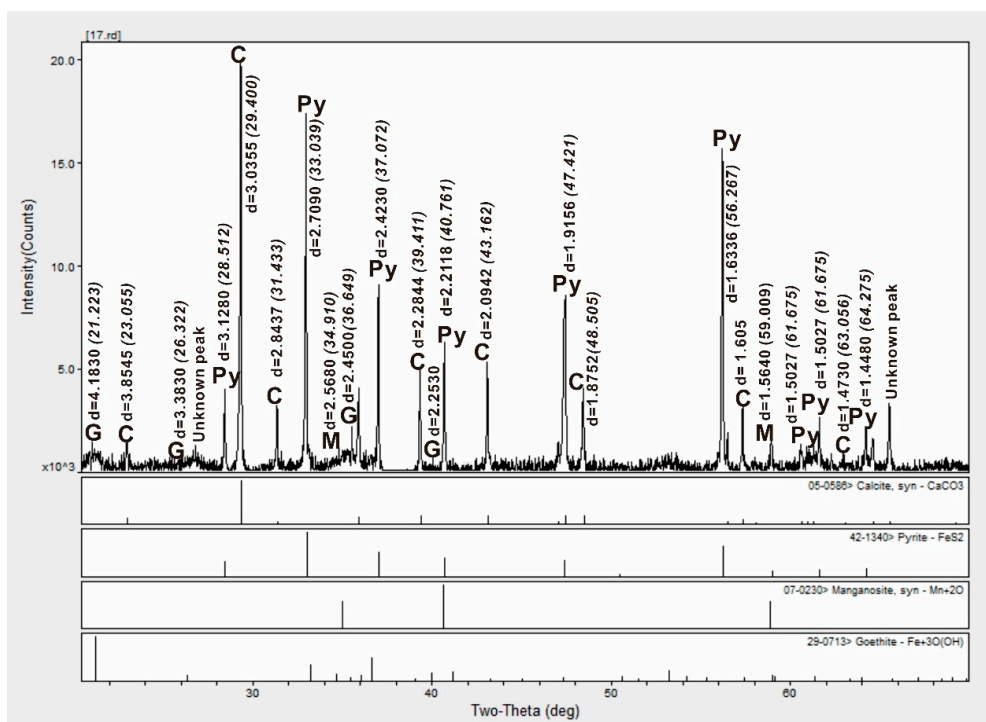
Figure 4. XRD patterns of the bulk sediment from station 28II-TVG05 (Wocan-2 site). Abbreviations, G: goethite; Sp: sphalerite; Py: pyrite; C: calcite; M: Manganosite. The 2θ values are enclosed in the bracket, whereas, the first values are the d values.
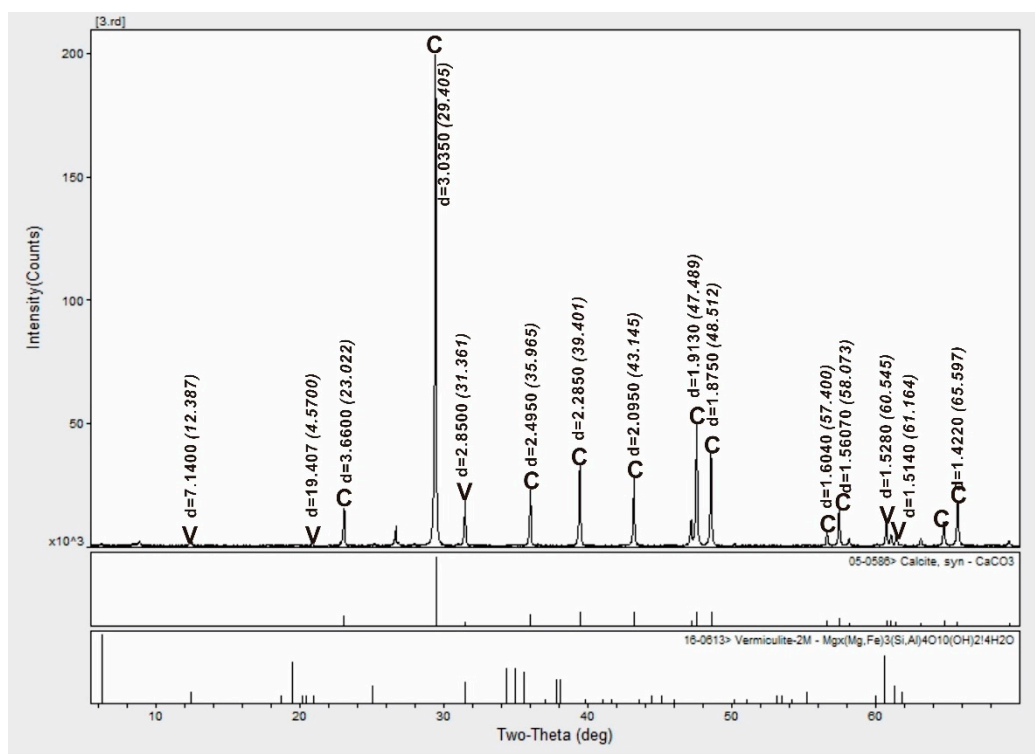

Figure 5. XRD patterns of the bulk sediment from station 28II-TVG13 (ridge flank). Abbreviations, C: calcite; V: vermiculite. The 2θ values are enclosed in the bracket, whereas, the first values are the d values.

**Table 2.** Relative abundance of Fe-oxyhydroxide separates from ~250–260 grain counts at the six stations.

Grain Counts	28I-TVG07	28I-TVG08	28I-TVG10	28II-TVG05	28I-TVG13	28I-TVG12
Fe-oxyhydroxide grains	132	139	176	119	29	13
Non-Fe-oxyhydroxide grains	122	118	87	132	219	233
Total grain counts	254	257	263	251	248	246
% Fe-oxyhydroxide	51.97	54.09	66.92	47.41	11.69	5.28

4.2. Morphology and Relative Abundance of Fe-Oxyhydroxide Separates

Fe-oxyhydroxide separates from Wocan-1 and Wocan-2 sites are poorly crystallized with a few angular to subangular texture (Figure 6A,B). Some are sub-rounded and botryoidal (Figure 6C,D). The Wocan-1 oxyhydroxides are majorly reddish-brown. While the oxyhydroxides of the Wocan-2 are reddish-brown to yellowish (Figure 7A), some primary sulfide grain separates exhibit features of partial oxidation into secondary iron-oxyhydroxides (Figure 7C). Others show inclusions of subangular to angular shards of S and Si-bearing of un-identified compounds (Figure 7B).
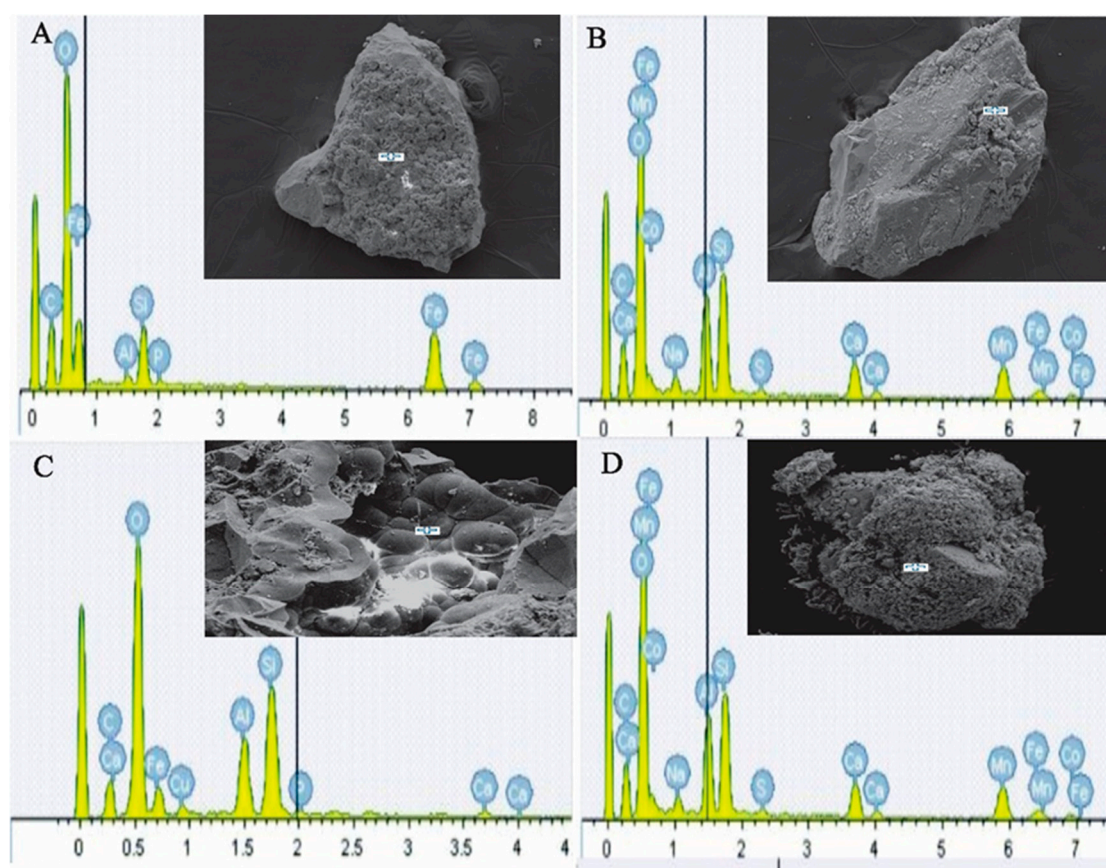
Figure 6. Representative SEM photomicrographs (secondary Electron Images (SEI) and EDS spectra on the morphology of Fe-Si-Mn oxyhydroxide (**A**) Angular Fe-Si-oxyhydroxide separate from the Wocan-1 samples (station 28I-TVG07). (**B**) Mn-enriched sub-angular Fe-oxyhydroxide separate from the Wocan-2 samples (station 28II-TVG05). (**C**) Micro-botryoidal morphology of typical Fe-oxyhydroxides separate from Wocan-2 samples (station 28I-TVG10). (**D**) Sub-rounded and botryoidal Mn-enriched oxyhydroxides from the ridge flanks (station 28I-TVG13). The cross sign represents the analyzed spot.
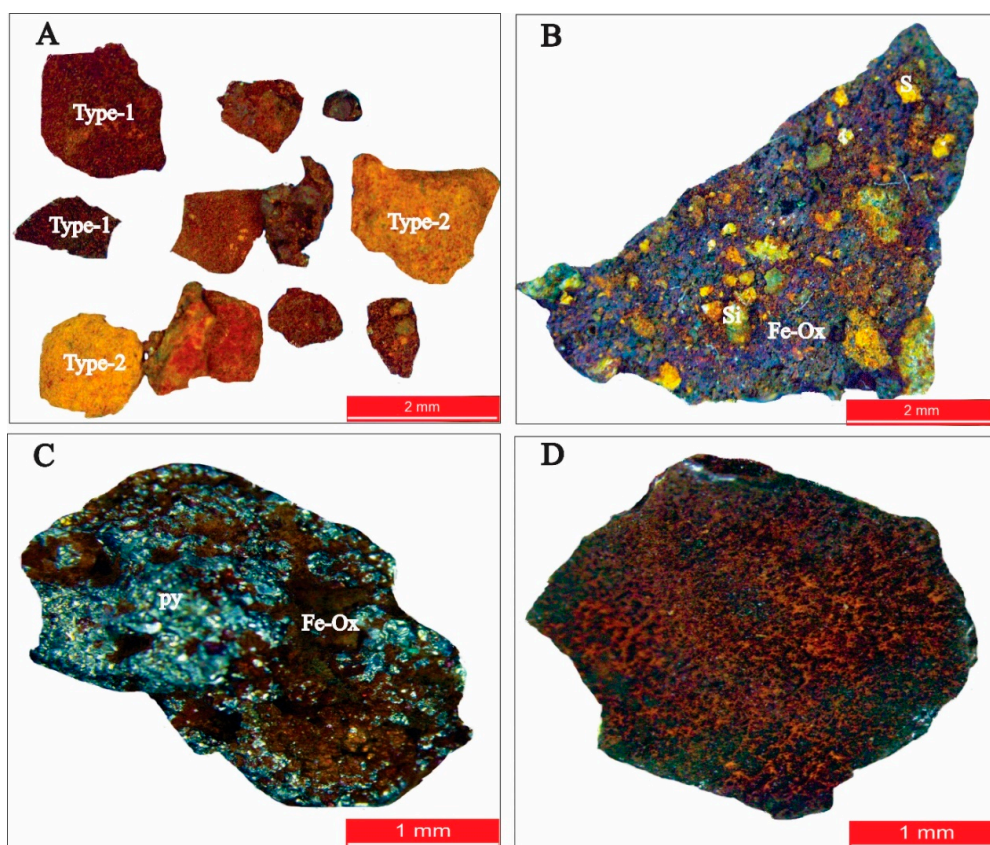
Figure 7. Photomicrographs of separated grains of Fe-oxyhydroxides. (**A**) A representative of reddish-brownish (type-1) and yellowish (type-2) angular to subangular Fe-oxyhydroxide separate. (**B**) Subangular to angular Si and S bearing phases in Fe-oxyhydroxide fragments. (**C**) Typical partially altered pyrite into secondary Fe-oxyhydroxide at station 28I-TVG10. (**D**) Typical sub-rounded reddish-brownish oxyhydroxide grains rich in Mn concentration at the Wocan-2 site (station 28I-TVG05), the emerald greenish-dark color suggests manganosite. Abbreviations, py: pyrite; Fe-ox: Fe-oxyhydroxides: Si: silica; S: sulfur.

The relative abundance of Fe-oxyhydroxide grains from ~250 to 260 counts (Table 2) shows up to ~54% and ~67% abundance on the Wocan-1 and Wocan-2 samples. The oxyhydroxides of the ridge flanks are less than 12%.

4.3. Mineral Chemistry of Fe-Oxyhydroxide Grains

In-situ geochemical investigations (using Electron Probe Microanalysis (EPMA) are essential tools in geochemical studies [27,28]. The improved methodology on spectrometers and efficient operations of the electron column at high probe current and acceleration voltage have increased the detection limit and precision of EPMA analysis to ppm levels [29]. References [15,30] applied EPMA on iron oxyhydroxide deposits from the Valu Fa Ridge, Lau Basin and PacMamus hydrothermal field, Eastern Manu Basin. The EPMA results of this study represent the average values of several analyses.

A total of 41 spots was investigated by EPMA on 35 representative Fe-oxyhydroxide grains separated from metalliferous sediment of WHF. The EPMA investigations on the Fe-oxyhydroxide separates of the Wocan-1 show Fe concentrations 49.05–55.14 wt. %, with variable Al_2O_3 (0.04–2.30 wt. %), TiO_2 (0.02–0.08 wt. %) and SiO_2 (6.85–16.31 wt. %) content. The Fe-oxyhydroxide separates show variable concentrations of minor elements which includes: BaO (0.02–0.11 wt. %); SrO (Bdl-0.05 wt. %); ZnO (0.41–0.92 wt. %); NiO (0.03–0.08 wt. %); PbO (0.06–0.19 wt. %) and CuO (0.55–1.38 wt. %). The mean sulfur content is 0.1 wt. % (n = 11, Table 3).

Table 3. Electron Probe Micro-analysis (wt. %) for Fe-Si-Mn oxyhydroxides from Wocan-1 site.

Element	SiO$_2$	SO$_3$	FeO	MnO	TiO$_2$	Al$_2$O$_3$	Al/(Al + Fe + Mn)	Fe/Mn			
Min	6.85	0.04	63.10	Bdl	0.02	0.04	0.0004	659.19			
Max	16.31	0.26	70.93	0.11	0.08	2.30	0.02	4,642.62			
Av	11.82	0.10	67.47	0.06	0.06	0.31	0.003	2,486.05			
STD-EV	±3.06	±0.08	±2.76	±0.05	±0.02	±0.67	±0.01	±66.06			
n = 11	**CuO**	**CoO**	**NiO**	**BaO**	**SrO**	**As$_2$O$_5$**	**ZnO**	**PbO**	**Total**	**H$_2$O$^+$ (calc)**	**Cu + Co + Zn + Ni**
Min	0.50	Bdl	0.03	0.02	Bdl	Bdl	0.41	0.06	71.11	28.89	0.79
Max	1.38	Bdl	0.08	0.11	0.05	0.15	0.92	0.19	93.35	6.65	1.78
Av	0.82	Bdl	0.05	0.05	0.02	0.06	0.64	0.10	81.72	18.28	1.19
STDEV	±0.26	-	±0.02	±0.04	±0.02	±0.04	±0.17	±0.04	±7.37	-	±0.31

STD-EV: standard deviation; Min: minimum; Max: maximum; Av: average.

The EPMA investigations of the reddish-brownish (type-1) and yellowish (type-2) Fe-oxyhydroxides of the Wocan-2 show distinct chemical compositions. The type-1 deposits have Fe concentrations of 49.31–55.12 wt. %, with variable Al$_2$O$_3$ (Bdl-1.96 wt. %), TiO$_2$ (0.03–0.09 wt. %) and SiO$_2$ (8.40–15.19 wt. %) content. The type-1 deposit shows variable concentrations of minor element which includes: BaO (Bdl-0.04 wt. %); SrO (Bdl-0.03 wt. %); ZnO (0.40–1.31 wt. %); NiO (Bdl-0.06 wt. %); PbO (0.02–0.10 wt. %) and CuO (0.52–1.41 wt. %) (n = 9, Table 4). The mean sulfur content (0.24 wt. %) is higher relative to Wocan-1 oxyhydroxides.

Table 4. Electron Probe Micro-analysis (wt. %) of type-1 Fe-Si-Mn oxyhydroxides from Wocan-2 site.

Element	SiO$_2$	SO$_3$	FeO	MnO	TiO$_2$	Al$_2$O$_3$	Al/(Al + Fe + Mn)	Fe/Mn			
Min	8.40	0.08	63.44	Bdl	0.03	Bdl	0.0002	1062			
Max	15.19	0.65	70.91	0.07	0.09	1.96	0.02	35,080			
Av	12.63	0.24	66.57	0.03	0.07	0.35	0.0036	9,557			
STD-EV	±2.07	±0.19	±2.63	±0.03	±0.03	±0.61	±0.006	±25.59			
n = 9	**CuO**	**CoO**	**NiO**	**BaO**	**SrO**	**As$_2$O$_5$**	**ZnO**	**PbO**	**Total**	**H$_2$O$^+$ (calc)**	**Cu + Co + Zn + Ni**
Min	0.52	Bdl	Bdl	Bdl	Bdl	Bdl	0.40	0.02	77.14	22.86	0.80
Max	1.41	Bdl	0.06	0.04	0.03	0.09	1.31	0.10	84.64	15.36	1.85
Av	0.89	Bdl	0.04	0.02	0.02	0.04	0.64	0.05	81.54	18.46	1.23
STD-EV	±0.26		±0.04	±0.01	±0.01	±0.03	±0.28	±0.04	±2.59	-	±0.36

STD-EV: standard deviation; Min: minimum; Max: maximum; Av: average.

The type-2 Fe-oxyhydroxides have lower Fe (6.69–20.69 wt. %) and higher SiO$_2$ (34.78–49.96 wt. %) contents. The S concentrations are bdl. The MnO, TiO$_2$ and Al$_2$O$_3$ contents are 0.07–0.35 wt. %; 0.09–5.46 wt. % and 0.07–19.08 wt. % (Table 5).

Table 5. Electron Probe Micro-analysis (wt. %) for type-2 Fe-Si-Mn oxyhydroxides from Wocan-2 site.

Element	SiO$_2$	SO$_3$	FeO	MnO	TiO$_2$	Al$_2$O$_3$	Al/(Al + Fe + Mn)	Fe/Mn			
Min	34.78	Bdl	8.60	0.07	0.09	0.07	0.003	25.81			
Max	49.96	Bdl	26.61	0.35	5.46	19.08	0.577	37.66			
Av	46.97	-	14.28	0.18	3.09	11.36	0.404	90.38			
STD-EV	±4.24	-	±4.30	±0.07	±2.13	±7.32	±0.20	±13.94			
n = 21	**CuO**	**CoO**	**NiO**	**BaO**	**SrO**	**AS$_2$O$_5$**	**ZnO**	**PbO**	**Total**	**H$_2$O$^+$ (calc)**	**Cu + Co + Zn + Ni**
Min	Bdl	Bdl	Bdl	Bdl	Bdl	Bdl	Bdl	Bdl	61.55	38.45	Bdl
Max	Bdl	Bdl	Bdl	Bdl	Bdl	Bdl	Bdl	Bdl	87.91	12.09	Bdl
Av	-	-	-	-	-	-	-	-	75.87	24.13	-
STD-EV	-	-	-	-	-	-	-	-	±10.49	-	-

STD-EV: standard deviation; Min: minimum; Max: maximum; Av: average.

Generally, the Wocan-1 Fe-oxyhydroxide show distinct enrichments in Ba, Sr, As and Pb, while, the type-1 Fe-oxyhydroxides of the Wocan-2 are enriched in Cu and Zn (Figure 8A,B). The minor element concentration of the type-2 Fe-oxyhydroxides is below detection limit.
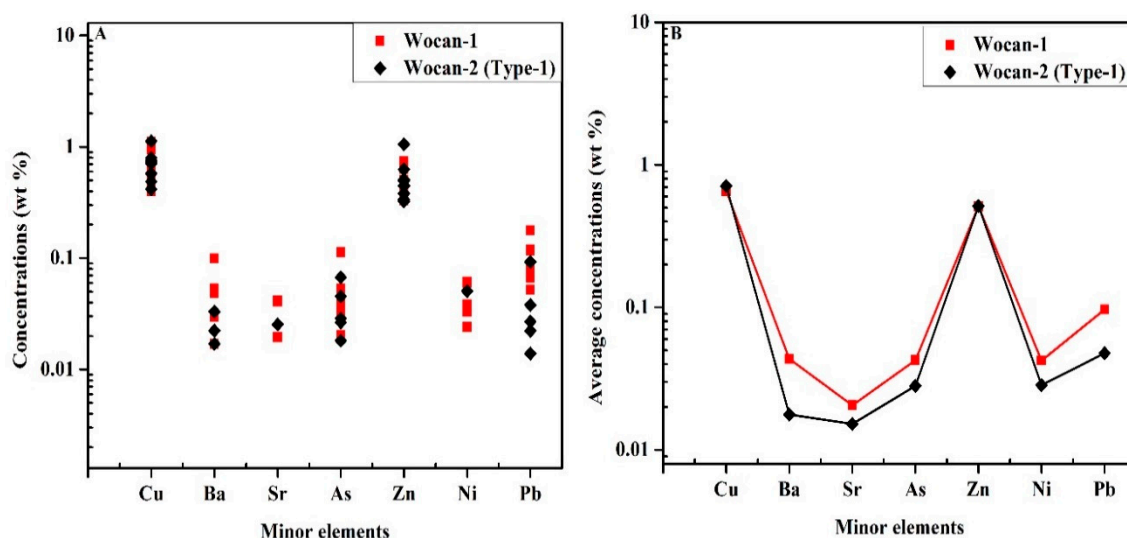
Figure 8. (**A**) Concentrations of the minor element (wt. %) in Fe-oxyhydroxide of Wocan-1 and type-1 Fe-oxyhydroxide of Wocan-2. (**B**) Average concentrations of the minor element in Wocan-1 Fe-oxyhydroxides and type-1 Fe-oxyhydroxides of Wocan-2 (n = 20).

The polishing of the ridge flank samples were difficult based on its friable nature, thereby creating some challenges on the EPMA investigation of the Mn-enriched oxyhydroxide grains (e.g., Figure 6D). Typical grains that resemble opaline silica (identified from the SEM and EDS spectrum) show high SiO_2 (81.09–92.35 wt. %) content, with low Fe (~0.02–0.07 wt. %) concentration. The MnO and BaO content is up to 5.11 wt. % and 0.05 wt. % respectively (Table 6, n = 3).

Table 6. Electron Probe Micro-analysis (wt. %) for typical Si-enriched grains from the ridge flanks.

Element	SiO_2	SO_3	FeO	MnO	TiO_2	Al_2O_3	Fe/Mn			
Min	81.09	Bdl	0.02	4.04	0.03	0.03	0.004			
Max	93.79	Bdl	0.09	5.11	0.08	0.58	0.022			
Av	89.08	-	0.05	4.75	0.05	0.43	0.011			
STD-EV	±6.42	-	±0.04	±0.54	0.03	±0.28	±0.01			

n = 3	CuO	CoO	NiO	BaO	SrO	AS_2O_5	ZnO	PbO	Total	Cu + Co + Zn + Ni
Min	Bdl	Bdl	Bdl	Bdl	Bdl	Bdl	Bdl	Bdl	86.83	Bdl
Max	Bdl	Bdl	Bdl	0.05	Bdl	Bdl	Bdl	Bdl	98.03	Bdl
Av	-	-	-	-	-	-	-	-	94.28	-
STD-EV	-	-	-	-	-	-	-	-	±5.70	-

STD-EV: standard deviation; Min: minimum; Max: maximum; Av: average.

The significantly lesser than 100% total of the EPMA analysis is probably due to evaporation of water from the samples under electron beam irradiation, similar to the reported values of [15,22,30]. We estimated the H_2O^+ concentrations from the summation of 100 according to [22].

5. Discussion

5.1. Origin and Formation Process of Wocan-1 Fe-Oxyhydroxides

Previous studies reported on three processes which gave rise to the Fe-oxyhydroxide deposits (i) The Fe-Si-Mn types that are predominantly formed by diffuse hydrothermal flow [3,12]. (ii) The Fe-Si-Mn types that are precipitated by seawater [31–34] and (iii) the Fe-Si-Mn types that are formed by mass wasting and corrosion of pre-existing sulfides [2,14]. However, these processes rarely occur in isolation and each may play an essential role in the precipitation of Fe-Mn oxyhydroxides at different stages [35,36]. The high metal content (e.g., Cu concentration >1 wt. %) collected from bottom-moored sediment traps (during the 2013 DY 28th cruise) [19] provided the direct evidence that the Fe-oxyhydroxide deposits on the Wocan-1 hydrothermal site are high-temperature hydrothermal precipitates.

Previous studies have utilized Fe/Ti and Al/(Al + Fe + Mn) ratios to estimate the hydrothermal and detrital contribution in metalliferous sediments and Fe-oxyhydroxides deposits [2,3,12,37–39]. Elevated Fe/Ti and low Al/(Al + Fe + Mn) ratio is an indication of strong hydrothermal components and enrichment of trace metals [39]. The increased Fe/Ti ratio and the low values of the Al/(Al + Fe + Mn) ratio (Figure 9) exhibited by the Wocan-1 Fe-oxyhydroxides are consistent with the enrichment of minor elements (Cu, Ba, Sr, As, Zn, Ni and Pb) in Figure 8.
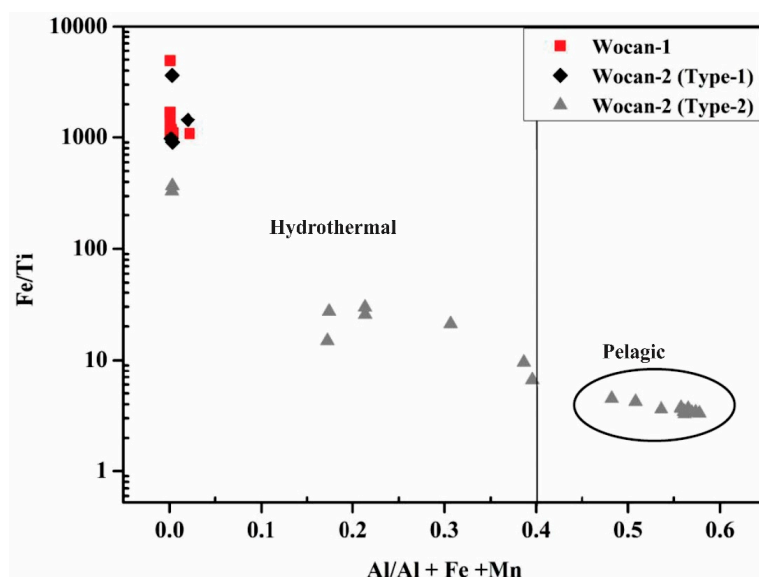

Figure 9. Ratios of Fe/Ti vs. Al/(Al + Fe + Mn) for Wocan-1 and Wocan-2 Fe-oxyhydroxides. The Al/(Al + Fe + Mn) values of some type-2 Fe-oxyhydroxide of Wocan-2 site are >0.40, an indications of detrital dilution of hydrothermal components [37].

Moreover, the identifications of sulfide mineral assemblage with the Fe-oxyhydroxides (Figure 3) and the plot of the Fe-rich corner of the Mn-Fe-(Cu + Co + Ni) × 10 ternary diagram (Figure 10), further indicates the hydrothermal origin and secondary sulfide oxidation.

Therefore, the high concentration of Fe (49.1–55.1 wt. %), transition metals other than Fe (0.79–1.78 wt. %) and S concentrations (mean value 0.10 wt. %) suggests that the Fe-oxyhydroxide deposits of the Wocan-1 belongs to the group-2 classifications from the detailed studies of [1,14,16]. This is an indication that the Wocan-1 Fe-oxyhydroxides are precipitated by mass wasting and corrosion of pre-existing sulfides (Figure 11).

Fe-oxyhydroxide deposits from the EPR 13°N, MESO (Central Indian Ocean Ridge) and the Mothra hydrothermal field (Endeavour segment, Juan de Fuca Ridge) have been linked to secondary alteration of pre-existing sulfide deposits [2,14,40,41].
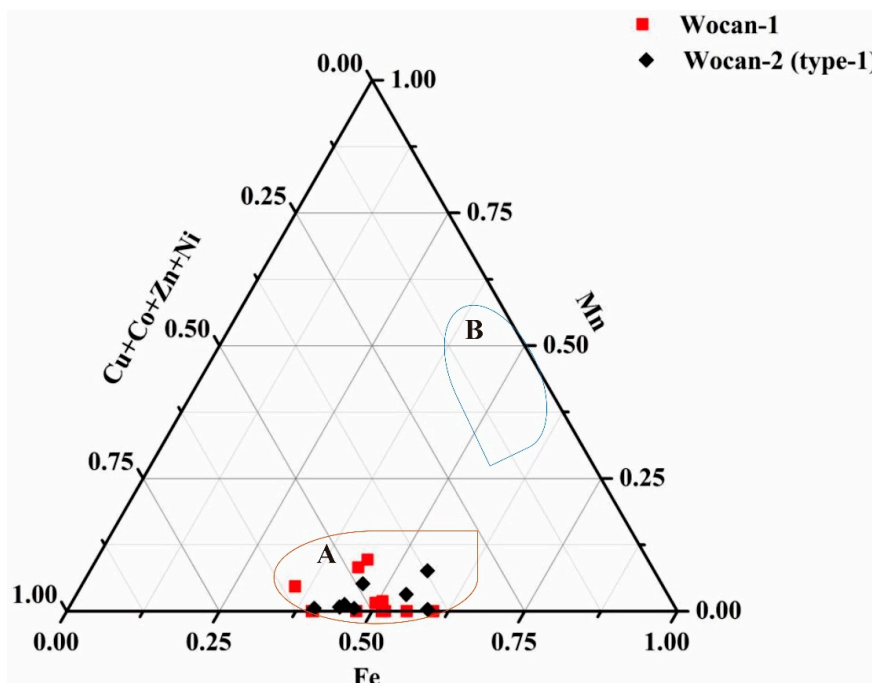
Figure 10. Mn-Fe-(Co + Ni + Cu) × 10 ternary diagram of Fe-oxyhydroxide deposits of: Wocan-1 and Wocan-2 type-1 Fe-oxyhydroxides. A indicates secondary sulfide oxidation origin after [14], B indicates diagenetic origin after [38].
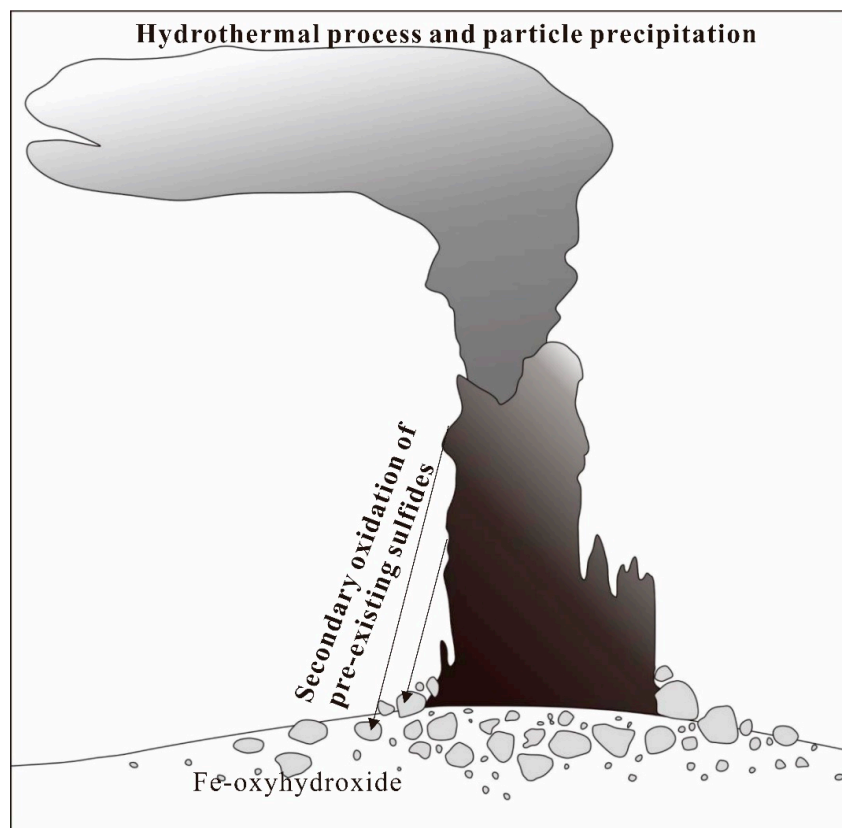

Figure 11. Schematic diagram showing the secondary oxidation of pre-existing sulfides in the Wocan hydrothermal site, modified after [14].

5.2. Origin and Formation Process of Wocan-2 Fe-Oxyhydroxides

Previous studies have reported the occurrence of an inactive toppled sulfide chimney in the vicinity of the Wocan-2 site, as an indication of previous widespread venting [19]. The lower values of Al/(Al + Fe + Mn) concentrations (mean value ~0.0036, n = 9) (Table 3), together with the Fe-rich corner of the Mn-Fe-(Cu + Co + Ni) × 10 ternary diagram (Figure 10) also support hydrothermal origin and secondary sulfide oxidation. The enriched transition metals (e.g., Cu + Co + Ni + Zn, mean value, 1.23 wt. %) further confirms these assumptions.

However, the regression plot (Figure 12) shows the existence of a weak relationship between the two typical oxyhydroxides (e.g., Wocan-1 and Wocan-2 type-1).
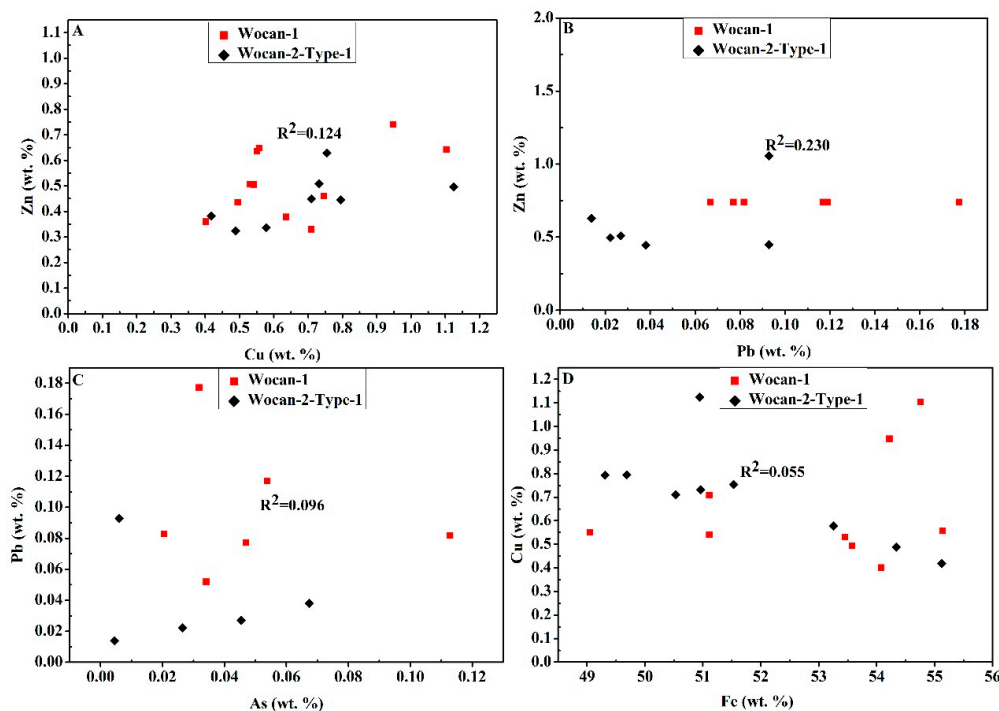
Figure 12. (**A–D**) The relationship between transition metals (Zn vs. Cu; Zn vs. Pb; Pb vs. As and Cu vs. Fe) of the Fe-oxyhydroxide deposits of the Wocan-1 and Wocan-2 (type-1). See Supplementary Materials for regression statistics.

The Zn contents show a weak correlation with Cu (R^2 = 0.124) and Pb (R^2 = 0.230) (Figure 12A,B). Also, the Pb vs. As (R^2 = 0.096) and Cu vs. Fe (R^2 = 0.053) show a similar weak relationship (Figure 12C,D). These weak correlations and strong probability values (P < 0.5) suggests a distinct geochemical process (e.g., high or low-temperature precipitates) between the two deposits.

The geochemical characteristics of the yellowish (type-2) Fe-oxyhydroxides suggest the increased influence of seawater on its precipitation. This assumption is supported by the depletion of minor element (Cu, Ba, Sr, As, Zn, Ni and Pb), and the higher Al/(Al + Fe + Mn) ratio (mean value 0.404). The Fe/Mn ratio (Tables 3–5) of the type-2 (Wocan-2) oxyhydroxides (25.87–37.66) is very low, relative to the type-1 (Wocan-2) 1062–3080 and Wocan-1 oxyhydroxides (69.19–4642). The low ratio is a further indication of seawater influence on its precipitation. Additionally, the low Fe/Ti and higher Al/(Al + Fe + Mn) values exhibited by the type-2 deposit (Figure 9) confirmed detrital dilution on the oxyhydroxides by deep sea pelagic types [37–39]. The observed Mn oxide minerals (Manganosite, Figure 4) further suggests its precipitation in an oxygenated environment relative to Wocan-1 and type-1 (Wocan-2) deposit. The Fe-oxyhydroxide deposit of station 28II-TVG05 displays these type-2 geochemical characteristics.

In comparison with the previous studies, the geochemical composition of the type-2 oxyhydroxides is similar to the group 3 classifications of [2,14].

5.3. Origin and Formation Process of Oxyhydroxide Separates of the Ridge Flanks

The low Fe/Mn ratio (0.004–0.022 mean value ~0.01) of the Si-Mn enriched grains and the depleted transition metal content suggest non-hydrothermal process on the formation of the ridge flanks oxyhydroxides. The Fe/Mn ratio is lower than the estimated value (<0.07) for hydrogenous Fe-Mn oxyhydroxide precipitates [36,41].

The sub-rounded Mn-enriched texture, with Ti, Ca and K inclusions in Figures 6D and 13A–E suggest the additional influence of pelagic oozes and terrigenous matter in the oxyhydroxides grains. These features indicate the absence of diffuse hydrothermal flow in the formation of the ridge flank oxyhydroxides [12].
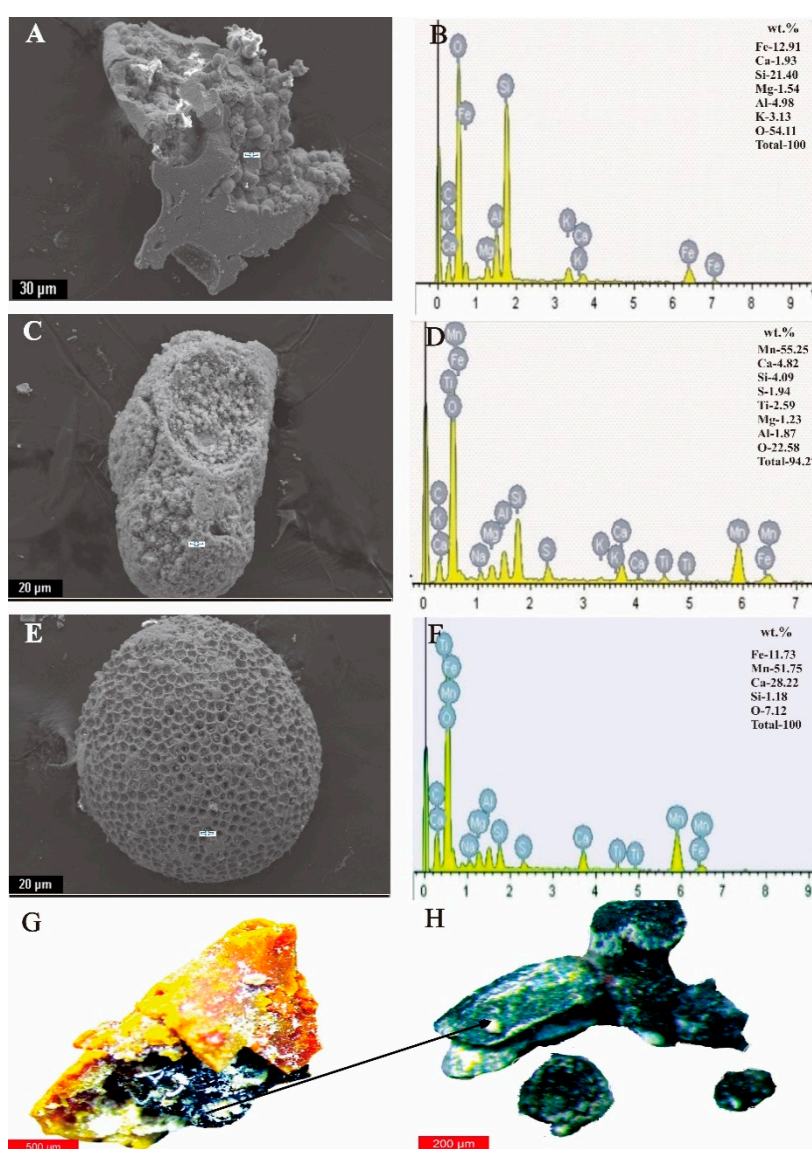
Figure 13. SEM photomicrographs and EDS spectra of (**A**–**F**) typical diagenetic alterations on the oxyhydroxides of the ridge flanks (**G**,**H**). An optical photomicrograph of typical biogenic influence on Mn oxyhydroxide precipitates. The SEM photomicrograph of G–H is shown in A and C, while the EDS spectra are in B and D. The cross sign represent analyzed spot.

The observed microbial mediated features from the optical microscope (Figure 13G,H) is an indication of microbial process in the precipitation of typical oxyhydroxide of the ridge flanks. Previous studies [42,43], have identified the existence of a spatial relationship between micro-organisms and the precipitation of Fe-oxyhydroxides in the hydrothermal environments and modern marine settings.

The geochemical composition of the ridge flanks Si-Mn oxyhydroxides (Table 6) are similar to the group 4 classification of [1,14].

6. Conclusions

Mineralogical investigations on the Fe-oxyhydroxide deposits of the Wocan-1 hydrothermal site highlighted their amorphous and poorly crystallized character. The X-Ray diffraction patterns of the bulk Fe-Si-Mn oxyhydroxides deposits on the Wocan-2 site show minor goethite and manganosite.

The morphology and geochemical investigations revealed two types of Fe-oxyhydroxide deposits at the Wocan hydrothermal sites (type-1 and type-2). The higher concentration of transition metals and the low Al/(Al + Fe + Mn) ratio of the type-1 oxyhydroxides suggest mass-wasting, corrosion and alterations of pre-existing sulfide minerals as the probable mode of formation. The depletion in transition metals, low Fe/Mn ratio and high Al/(Al + Fe + Mn) values of the type-2 Fe-oxyhydroxides suggest an increased contribution of sea water during the process of secondary sulfide oxidation.

The presence of biogenic mediated Mn-rich oxyhydroxide precipitates, low Fe/Mn ratio and depletion in transition metals suggest mixed (diagenetic and hydrogenous) origin to the ridge flank oxyhydroxides.

Our results further indicate a marked shift from reduced to oxygenated environments in the precipitation of Fe-oxyhydroxides with distance from hydrothermal sites.

References

1. Hekinian, R.; Hoffert, M.; Larqué, P.; Cheminée, J.L.; Stoffers, P.; Bideau, D. Hydrothermal Fe and Si oxyhydroxide deposits from South Pacific intraplate volcanoes and East Pacific Rise axial and off-axial regions. *Econ. Geol.* **1993**, *88*, 2099–2121. [CrossRef]

2. Hrischeva, E.; Scott, S.D. Geochemistry and morphology of metalliferous sediments and oxyhydroxides from the Endeavour segment, Juan de Fuca Ridge. *Geochim. Cosmochim. Acta* **2007**, *71*, 3476–3497. [CrossRef]

3. Dekov, V.M.; Petersen, S.; Garbe-Schönberg, C.D.; Kamenov, G.D.; Perner, M.; Kuzmann, E.; Schmidt, M. Fe-Si-oxyhydroxide deposits at a slow-spreading centre with thickened oceanic crust: The Lilliput hydrothermal field (9°33′S, Mid-Atlantic Ridge). *Chem. Geol.* **2010**, *278*, 186–200. [CrossRef]

4. Fouquet, Y.; von Stackelberg, U.; Charlou, J.L.; Donval, J.L.; Erzinger, J.; Foucher, J.P.; Herzig, P.; Muhe, R.; Soakai, S.; Wiedicke, M. Metallogenesis in back-arc environments: The Lau Basin example. *Econ. Geol.* **1993**, *88*, 2154–2181. [CrossRef]

5. Lizasa, K.; Kawasaki, K.; Maeda, K.; Matsumoto, T.; Saito, N.; Hirai, K. Hydrothermal sulfide-bearing Fe-Si oxyhydroxide deposits from the Coriolis Troughs, Vanuatu backarc, southwestern Pacific. *Mar. Geol.* **1998**, *145*, 1–21.

6. Dekov, V.; Savelli, C. Hydrothermal activity in the SE Tyrrhenian Sea: An overview of 30 years of research. *Mar. Geol.* **2004**, *204*, 161–185. [CrossRef]

7. Kato, S.; Kobayashi, C.; Kakegawa, T.; Yamagishi, A. Microbial communities in iron-silica-rich microbial mats at deep-sea hydrothermal fields of the Southern Mariana Trough. *Environ. Microbiol.* **2009**, *11*, 2094–2111. [CrossRef]

8. Alt, J.C.; Lonsdale, P.; Haymon, R.; Muehlenbachs, K. Hydrothermal sulfide and oxide deposits on seamounts near 21°N, East Pacific Rise. *Geol. Soc. Am. Bull.* **1987**, *98*, 157–168. [CrossRef]

9. Boyd, T.D.; Scott, S.D. Two-XRD-line ferrihydrite and Fe-Si-Mn oxyhydroxide mineralization from Franklin Seamount, western Woodlark Basin, Papua New Guinea. *Can. Miner.* **1999**, *37*, 973–990.

10. Dekov, V.M.; Kamenov, G.D.; Savelli, C.; Stummeyer, J.; Thirye, M.; Shanks, W.C.; Willingham, A.L.; Boycheva, T.B.; Rochette, P.; Kuzmann, E.; et al. Metalliferous sediments from Eolo Seamount (Tyrrhenian Sea): Hydrothermal deposition and re-deposition in a zone of oxygen depletion. *Chem. Geol.* **2009**, *264*, 347–363. [CrossRef]

11. Hein, J.R.; Schulz, M.S.; Dunham, R.E.; Stern, R.J.; Bloomer, S.H. Diffuse flow hydrothermal manganese mineralization along the active Mariana and southern Izu-Bonin arc system, western Pacific. *J. Geophys. Res.* **2008**, *113*, Bo8S14. [CrossRef]

12. Sun, Z.; Zhou, H.; Yang, Q.; Sun, Z.; Bao, S.; Yao, H. Hydrothermal Fe-Si-Mn oxide deposits from the Central and South Valu Fa Ridge, Lau Basin. *Appl. Geochem.* **2011**, *26*, 1192–1204. [CrossRef]

13. Mills, R.A.; Elderfield, H. Rare Earth Element geochemistry of hydrothermal deposits from the active TAG Mound 26°N Mid-Atlantic Ridge. *Geochem. Cosmochim. Acta* **1995**, *59*, 3511–3524. [CrossRef]

14. Zeng, Z.; Wang, X.; Zhang, G.; Yin, X.; Chen, D.; Wang, X. Formation of Fe-oxyhydroxides from the East Pacific Rise near latitude 13°N: Evidence from mineralogical and geochemical data. *Sci. China Ser. D Earth Sci.* **2008**, *51*, 206–215. [CrossRef]

15. Zeng, Z.; Chen, S.; Wang, X.; Ouyang, H.; Yin, X.; Li, Z. Mineralogical and micromorphological characteristics of Si-Fe-Mn oxyhydroxides from the PACMANUS hydrothermal field, Eastern Manus Basin. *Sci. China Earth Sci.* **2012**, *55*, 2039–2048. [CrossRef]

16. Hekinian, R. *Hydrothermal Activity and Metalliferous Deposits, Sea Floor Exploration: Scientific Adventures Diving into the Abyss*; Springer International Publishing: Cham, Switzerland, 2014; pp. 145–164.

17. Marchig, V.; Gundlach, H.; Moller, P.; Schley, F. Some geochemical indicators for discrimination between diagenetic and hydrothermal metalliferous sediments. *Mar. Geol.* **1982**, *50*, 241–256. [CrossRef]

18. Sun, Z.; Li, J.; Huang, W.; Dong, H.; Little, C.T.S.; Li, J. Generation of hydrothermal Fe-Si oxyhydroxide deposit on the Southwest Indian Ridge and its implication for the origin of ancient banded iron formations. *J. Geophys. Res. Biogeosci.* **2015**, *120*, 187–203. [CrossRef]

19. Wang, Y.; Han, X.; Petersen, S.; Frische, M.; Qiu, Z.; Li, H.; Li, H.; Wu, Z.; Cui, R. Mineralogy and trace element geochemistry of sulfide minerals from the Wocan Hydrothermal Field on the slow-spreading Carlsberg Ridge, Indian Ocean. *Ore Geol. Rev.* **2017**, *84*, 1–19. [CrossRef]

20. Murton, B.J.; Rona, P.A. Carlsberg ridge and mid-Atlantic ridge: Comparison of slow spreading centre analogues. *Deep Sea Res.* **2015**, *121*, 71–84. [CrossRef]

21. Dias, Á.S.; Mills, R.A.; Taylor, R.N.; Ferreira, P.; Barriga, F.J.A.S. Geochemistry of a sediment push-core from the Lucky Strike hydrothermal field, Mid-Atlantic Ridge. *Chem Geol.* **2008**, *247*, 339–351. [CrossRef]

22. Mohapatra, B.K.; Jena, S.; Singh, P.P. Microstructure-compositional variation in iron oxy-hydroxide minerals formed with manganese mineralization, Eastern Ghats Supergroup, Orissa. *J. Geol. Soc. India* **2011**, *77*, 450–458. [CrossRef]

23. Mange, M.A.; Maurer, H.F.W. *Methods, Heavy Minerals in Colour*; Springer: Dordrecht, The Netherlands, 1992; pp. 11–25.

24. Ramdohr, P. Goethite from Hind low, Derbyshire. *Bull. Geol. Surv. G. B.* **1980**, *52*, 51–54. Available online: http://handbookofmineralogy.org/pdfs/manganosite (accessed on 28 November 2018).

25. Criddle, A.J.; Stanley, C.J. (Eds.) *Quantitative Data File for Ore Minerals*, 3rd ed.; Chapman & Hall: London, UK, 1955; Volume 351, Available online: http://handbookofmineralogy.org/pdfs/Goethite (accessed on 28 November 2018).

26. Popoola, S.O.; Han, X.; Wang, Y.; Qiu, Z.; Cai, Y. Mineralogical and geochemical signature of metalliferous sediments in Wocan-1 and Wocan-2 hydrothermal sites, on the Carlsberg Ridge, Indian Ocean. *Mineral* **2018**. submitted.

27. Cook, N.J.; Ciobanu, C.L.; Ehrig, K.; Slattery, A.; Verdugo-Ihl, M.R.; Courtney-Davies, L.; Gao, W. Advances and Opportunities in Ore Mineralogy. *Minerals* **2017**, *7*, 233. [CrossRef]
28. Reich, M.; Large, R.; Deditius, A.P. New advances in trace element geochemistry of ore minerals and accessory phases. *Ore Geol. Rev.* **2017**, *81*, 1215–1217. [CrossRef]
29. Batanova, V.G.; Sobolev, A.V.; Magnin, V. Trace element analysis by EPMA in geosciences: Detection limit, precision and accuracy. *IOP Conf. Ser. Mater. Sci. Eng.* **2018**, *304*, 012001. [CrossRef]
30. Sun, Z.; Zhou, H.; Glasby, G.P.; Sun, Z.; Yang, Q.; Yin, X.; Li, J. Mineralogical characterization and formation of Fe-Si oxyhydroxide deposits from modern seafloor hydrothermal vents. *Am. Mineral.* **2013**, 85–97. [CrossRef]
31. Benites, M.; Millo, C.; Hein, J.; Nath, B.N.; Murton, B.; Galante, D.; Jovane, L. Integrated Geochemical and Morphological Data Provide Insights into the Genesis of Ferromanganese Nodules. *Minerals* **2018**, *8*, 488. [CrossRef]
32. Yeo, I.A.; Dobson, K.; Josso, P.; Pearce, R.B.; Howarth, S.A.; Lusty, P.A.J.; Le Bas, T.P.; Murton, B.J. Assessment of the Mineral Resource Potential of Atlantic Ferromanganese Crusts Based on Their Growth History, Microstructure, and Texture. *Minerals* **2018**, *8*, 327. [CrossRef]
33. Marino, E.; González, F.J.; Lunar, R.; Reyes, J.; Medialdea, T.; Castillo-Carrión, M.; Bellido, E.; Somoza, L. High-Resolution Analysis of Critical Minerals and Elements in Fe-Mn Crusts from the Canary Island Seamount Province (Atlantic Ocean). *Minerals* **2018**, *8*, 285. [CrossRef]
34. Halbach, P. Processes controlling the heavy metal distribution in Pacific ferromanganese nodules and crusts. *Geologische Rundschau* **1986**, *75*, 235–247. [CrossRef]
35. Varentsov, I.M.; Drits, V.A.; Gorshkov, A.I.; Sivtsov, A.V.; Sakharov, B.A. Mn-Fe oxyhydroxide crusts from Krylov Seamount (Eastern Atlantic): Mineralogy, geochemistry and genesis. *Mar. Geol.* **1991**, *96*, 53–70. [CrossRef]
36. Wang, X.; Zeng, Z.; Qi, H.; Chen, S.; Yin, X.; Yang, B. Fe-Si-Mn-oxyhydroxide encrustations on basalts at East Pacific Rise near 13°N: An SEM-EDS study. *J. Ocean Univ. China* **2014**, *13*, 917–925. [CrossRef]
37. Boström, K. The origin and fate of ferromanganoan active ridge sediments. *Stock. Contrib. Geol.* **1973**, *27*, 149–243.
38. Bonatti, E. Metal deposits in the oceanic lithosphere. In *The Sea*; Emiliani, C., Ed.; John Willey and Sons: New York, NY, USA, 1981; Volume 7, pp. 639–686.
39. Dias, Á.S.; Barriga, F.J.A.S. Mineralogy and geochemistry of hydrothermal sediments from the serpentinite-hosted Saldanha hydrothermal field (36°34′N; 33°26′W) at MAR. *Mar. Geol.* **2006**, *225*, 157–175. [CrossRef]
40. Münch, U.; Blum, N.; Halbach, P. Mineralogical and geochemical features of sulfide chimneys from the MESO zone, Central Indian Ridge. *Chem. Geol.* **1999**, *155*, 29–44. [CrossRef]
41. Moorby, S.A.; Cronan, D.S.; Glasby, G.P. Geochemistry of hydrothermal Mn oxide deposits from the SW Pacific island arc. *Geochim. Cosmochim. Acta* **1984**, *48*, 433–441. [CrossRef]
42. Kennedy, C.B.; Martinez, R.E.; Scott, S.D.; Ferris, F.G. Surface chemistry and reactivity of bacteriogenic iron oxides from Axial Volcano, Juan de Fuca Ridge, north-east Pacific Ocean. *Geobiology* **2003**, *1*, 59–69. [CrossRef]
43. Tsikos, H.; Matthews, A.; Erel, Y.; Moore, J.M. Iron isotopes constrain biogeochemical redox cycling of iron and manganese in a Palaeoproterozoic stratified basin. *Earth Planet. Sci. Lett.* **2010**, *298*, 125–134. [CrossRef]